arXiv:1702.01386v1 [cs.IT] 5 Feb 2017

Joint DOA and Frequency Estimation with Sub-Nyquist Sampling for More Sources than Sensors

Liang Liu and Ping Wei

***Abstract*—In this letter, we apply previous array receiver architecture which employs time-domain sub-Nyquist sampling techniques to jointly estimate frequency and direction-of-arrival(DOA) of narrowband far-field signals. Herein, a more general situation is taken into consideration, where there may be more than one signal in a subband. We build time-space union model, analyze the identification of the model, and give the maximum signal number which can be classified. We also proof that the Cramér-Rao Bound (CRB) is lower than that of which employs Nyquist sampling. Simulation results verify the capacity to estimate the number of sources. Meanwhile, simulations show that our estimation performance closely matches the CRB and is superior for more sources than sensors, especially when the minimum redundancy array (MRA) is employed.**

***Index Terms*—Direction-of-arrival estimation, frequency estimation, sub-Nyquist sampling, Cramér-Rao Bound.**

I. Introduction

TO better deal with the problem of the spectral congestion [1]–[5], Cognitive Radio (CR) technique consider three main spectrum, i.e., time, frequency and space, to improve access possibility. The development of array processing techniques [6]–[8] provides a spatial spectrum access opportunity to increase the spectral resource utilization. Since space-time spectrum sensing need to make full use of spectral resource, jointly estimate carrier frequency and direction-of-arrival(DOA) [9], [10] is main challenge. There are two dramatical shortcomings of the existing methods. One is the pair matching problem between the carrier frequencies and the DOAs. The other is that the Nyquist sampling is too high for wideband signal processing, which becomes a bottleneck for CRs. Typically, it is intolerable due to of the too high Nyquist sampling rate or too much data to process when the monitoring range is from 300 MHz to several GHz [1]–[5].

Recent years, sub-Nyquist sampling technique has been widely researched to reconstruct a multiband signal from the data obtained under the Nyquist sampling rate [11]–[14]. Inspired by the idea, some joint estimation methods of DOA and carrier frequency were proposed for the under Nyquist sampling rate situation. The authors of [15] suggested a new structure, where each output of a linear array employs the multi-coset sampling. If the array is a nonuniform linear array, the signal can be compressed in both the time domain and spatial domain. [16] use only one additional identical delayed channel for each antenna to simplify the hardware complexity. Herein, the mismatch problem will happen when using an underlying uniform linear array (ULA). To this end, the authors proposed another structure in [17], which still has low hardware complexity. In [18], the authors proposed the so-called space-time array to jointly estimate frequency and DOA when the number of sources is more than the number of sensors. More recently, two joint DOA and carrier frequency recovery approaches based on the L-shaped ULAs were presented in [19]. In [20], a receiver architecture and estimation algorithms is proposed to jointly estimate frequency and DOA. However, merely a special situation is considered in [20], where there is at most one signal in a subband.

Based on the receiver architecture proposed in [20], this letter considers a more general situation, where there may exist more than one narrowband far-field signal in a subband. We built the time-space union model for this scenario. After analyzing the identification of the model, the maximum signal number which can be classified is given. The proposed model is capable of estimating more signals than sensors. We also proof that the Cramér-Rao Bound (CRB) is lower than that which employing Nyquist sampling. The simulation verifies the capacity to estimate the number of sources. Besides, simulation shows that our estimation performance closely matches the CRB and is superior for more sources than sensors, especially when the minimum redundancy array (MRA) is employed.

II. Signal model and objective

Consider K narrowband far-field signals $\mathbf{s}(t) = [s_1(t), \cdots, s_K(t)]^{\mathrm{T}}$ impinging on a ULA composed of M sensors, where $(\cdot)^{\mathrm{T}}$ denotes the transpose. It should be noted that arbitrary array form can be employed as explained in [20]. The frequency domain array output can be written as [6]

$$\mathbf{X}(f) = \mathbf{A}\mathbf{S}(f) + \mathbf{N}(f), \tag{1}$$

where $A_{mk} = \exp(-j\phi_k(m-1))$ is the (m,k)th element of the steer array. The spatial phase is shown as

$$\phi_k = \frac{\pi d \sin(\theta_k) f_k}{f_N}, \tag{2}$$

where d is the distance between two consecutive antennas in half-wavelengths corresponding to the Nyquist sampling rate f_N. θ_k and f_k are the DOA and the

The authors are with the Center for Cyber Security, School of Electronic Engineering, University of Electronic Science and Technology of China, Chengdu, 611731 China (e-mail:liu_yinliang@outlook.com; pwei@uestc.edu.cn).

center frequency of $s_k(t)$, respectively. The sensor position vector is $\mathbf{d} = [0, 1, \cdots, M-1]\, d$. $\mathbf{X}(f) = [X_1(f), \cdots, X_M(f)]^{\mathrm{T}}$, $\mathbf{S}(f) = [S_1(f), \cdots, S_K(f)]^{\mathrm{T}}$, and $\mathbf{N}(f) = [N_1(f), \cdots, N_M(f)]^{\mathrm{T}}$ are the frequency domain expression of $\mathbf{x}(t)$, $\mathbf{s}(t)$, $\mathbf{n}(t)$, respectively. $X_m(f)$ is the Fourier transform of $x_m(t)$. The measurement vector and the noise vector are defined as $\mathbf{x}(t) = [x_1(t), \cdots, x_M(t)]^{\mathrm{T}}$ and $\mathbf{n}(t) = [n_1(t), \cdots, n_M(t)]^{\mathrm{T}}$, respectively. The noise subjects to the zero-mean complex spatially and temporarily white Gaussian distribution with covariance matrix $\sigma^2\mathbf{I}_M$, where $\mathbf{I}_M$ stands for an $M \times M$ identity matrix.

The objective of this letter is to simultaneously estimate the carrier frequency f_k and DOA θ_k of multiple signals $s_k(t)$ under the Nyquist sampling rate.

III. Signal reception model and Identification

A. Signal reception model

We employ the receiver architecture as Fig. 1 in [20]. There are M sensors and every sensor is followed by P delay branches in the architecture. $f_{sub} = f_N/L$ is the sub-Nyquist sampling rate, where L is the sampling rate reduction factor and $y_{mp}[n]$ denotes the sampled signal corresponding to the mth sensor, pth branch. The sampling pattern is set at $C = [c_1, c_2, \cdots, c_P]$. In (1), suppose that column order of $\mathbf{A}$ is determined by the frequency of signals, and there are K_l signals in lth subband. The following notations are introduced: $\mathbf{S}^{\mathrm{T}}(f) = \left[\mathbf{S}_1^{\mathrm{T}}(f), \cdots, \mathbf{S}_L^{\mathrm{T}}(f)\right] \in C^{1\times K}$, $\mathbf{S}_l^{\mathrm{T}}(f) = [S_{l1}(f), \cdots, S_{lK_l}(f)] \in C^{1\times K_l}$, $f \in \left[0, \frac{1}{T}\right)$, $K = \sum_{l=1}^{L} K_l$, where $\mathbf{S}_l(f)$ refer to all the signals in the lth subband, $S_{lk}(f)$ is the kth signal in the lth subband. The steel vector will be $\mathbf{A} = [\mathbf{A}_1, \cdots, \mathbf{A}_L] \in C^{M\times K}$, $\mathbf{A}_l = \left[(\mathbf{A}_l)_1, \cdots, (\mathbf{A}_l)_{K_l}\right] \in C^{M\times K_l}$, where $\mathbf{A}_l$ is the steel matrix corresponding to $\mathbf{S}_l(f)$ as well as the lth block of $\mathbf{A}$, and $(\mathbf{A}_l)_k$ is the steel vector corresponding to $S_{lk}(f)$ as well as the kth column of $(\mathbf{A}_l)$.

According to (1), the output of the mth sensor is

$$X_m(f) = \mathbf{A}^m\mathbf{S}(f) + N_m(f), f \in \left[0, \frac{1}{T_N}\right), \tag{3}$$

where $\mathbf{A}^m = [(\mathbf{A}_1)^m, \cdots, (\mathbf{A}_L)^m]$ is the mth row of $\mathbf{A}$. Combining the conclusions of [14], [20], the output of all branches of mth sensor is expressed as

$$\mathbf{Y}_m(f) = \mathbf{B}\overline{\mathbf{X}}_m(f), f \in \mathcal{F} \tag{4}$$

where $B_{il} = \frac{1}{\sqrt{L}}\exp\left(j\frac{2\pi}{L}c_i l\right)$, $\mathbf{Y}_m(f) = \sqrt{L}T_N\left[Y_{m1}\left(e^{j2\pi f T_N}\right), \cdots, Y_{mP}\left(e^{j2\pi f T_N}\right)\right]^{\mathrm{T}}$, $\overline{\mathbf{X}}_m(f) = [X_{m1}(f), \cdots, X_{mL}(f)]^{\mathrm{T}}$, $X_{ml}(f) = X_m(f + (l-1)f_{sub})$, $\mathcal{F} \triangleq [0, f_{sub})$. $T_N = 1/f_N$ is the Nyquist sampling interval. $Y_{mp}\left(e^{j2\pi f T_N}\right)$ is the discrete-time Fourier transform of $y_{mp}[n]$. Based on (3) and the form of $\overline{\mathbf{X}}_m(f)$, we have

$$\overline{\mathbf{X}}_m(f) = \mathrm{blkdiag}\left((\mathbf{A}_1)^m, \cdots, (\mathbf{A}_L)^m\right)\overline{\mathbf{S}}(f) + \overline{\mathbf{N}}_m(f), \quad f \in \mathcal{F}, \tag{5}$$

where $\overline{\mathbf{S}}^{\mathrm{T}}(f) = \left[\overline{\mathbf{S}}_1^{\mathrm{T}}(f), \cdots, \overline{\mathbf{S}}_L^{\mathrm{T}}(f)\right]$, $\overline{\mathbf{S}}_l^{\mathrm{T}}(f) = \left[\overline{S}_{l1}(f), \cdots, \overline{S}_{lK_l}(f)\right]$, $\overline{S}_{lk}(f) = S_{lk}(f + (l-1)f_{sub})$, $\overline{\mathbf{N}}_m(f) = \left[\overline{N}_{m1}(f), \cdots, \overline{N}_{mL}(f)\right]^{\mathrm{T}}$, $\overline{N}_{ml}(f) = N_m(f + (l-1)f_{sub})$. $\mathrm{blkdiag}(\mathbf{z}_1, \cdots, \mathbf{z}_m)$ represents a block diagonal matrix with diagonal entries $\mathbf{z}_1, \cdots, \mathbf{z}_m$. Substituting (5) into (4), we get

$$\begin{aligned}\mathbf{Y}_m(f) =& \mathbf{B}\mathrm{blkdiag}\left((\mathbf{A}_1)^m, \cdots, (\mathbf{A}_L)^m\right)\overline{\mathbf{S}}(f) + \mathbf{B}\overline{\mathbf{N}}_m(f) \\ =& \left[(\mathbf{A}_1)^m \otimes \mathbf{B}_1, \cdots, (\mathbf{A}_L)^m \otimes \mathbf{B}_L\right]\overline{\mathbf{S}}(f) \\ &+ \mathbf{B}\overline{\mathbf{N}}_m(f), f \in \mathcal{F}\end{aligned} \tag{6}$$

where $\overline{\mathbf{S}}(f) = \left[\overline{\mathbf{S}}_1^{\mathrm{T}}(f), \cdots, \overline{\mathbf{S}}_K^{\mathrm{T}}(f)\right]^{\mathrm{T}}$, $\overline{\mathbf{S}}_k(f) = [S_{k1}(f), \cdots, S_{kL}(f)]^{\mathrm{T}}$. $\otimes$ denotes the Kronecker product. Then, combining all m can result in

$$\begin{aligned}\mathbf{Y}(f) =& \left[\mathbf{A}_1 \otimes \mathbf{B}_1, \cdots, \mathbf{A}_L \otimes \mathbf{B}_L\right]\overline{\mathbf{S}}(f) + \left(\mathbf{I}_M \otimes \mathbf{B}\right)\overline{\mathbf{N}}(f), \\ =& \mathbf{G}\overline{\mathbf{S}}(f) + \mathbf{I}_{\mathbf{B}}\overline{\mathbf{N}}(f), f \in \mathcal{F}\end{aligned} \tag{7}$$

where $\mathbf{Y}(f) = \left[\mathbf{Y}_1^{\mathrm{T}}(f), \cdots, \mathbf{Y}_M^{\mathrm{T}}(f)\right]^{\mathrm{T}}$, $\overline{\mathbf{N}}(f) = \left[\overline{\mathbf{N}}_1(f), \cdots, \overline{\mathbf{N}}_L(f)\right]$. Actually, $\mathbf{Y}(f)$ in (7) is the matrix form of the output of all branches of all sensors.

After modeling the reception model, we can apply JDFSD in [20] to solve it. The difference between the two papers is that there maybe be one or more signals in one subband in this paper while there is at most one signal in one subband in [20]. Therefore, the method in this paper is named JDFSD4MU.

B. Identification

For identification, only consider a simple situation: the branch number is equal to the sampling rate reduction factor ($P = L$), and there are no more than $M-1$ signals in each subband, which are from different DOAs. So we have $Rank(\mathbf{V}_i) = Rank(\mathbf{A}_i) = K_i$, where $\mathbf{V}_i = \mathbf{A}_i \otimes \mathbf{B}_i$. $Rank(\cdot)$ denotes the rank of a matrix. Apparently, we will hold $\mathbf{V}_i \perp \mathbf{V}_j, i \neq j$, since $\mathbf{B}^{\mathrm{H}}\mathbf{B} = \mathbf{I}$ when $P = L$. Further, we get $Rank(\mathbf{G}) = \sum_{i=1}^{L} Rank(\mathbf{V}_i) = K$. Based on the subspace decomposition theory [7] and $Rank(\mathbf{G}) = K$, the model (7) can be solved and the maximum signal number which can be classified is $(M-1)L$.

IV. Cramér-Rao Bound

Based on [20], the CRB of our model is given by

$$\mathrm{CRB}_{sub} = \frac{\sigma^2}{2T}\left(\Re\left(\left(\mathbf{E}^{\mathrm{H}}\mathbf{P}_{\mathbf{G}}\mathbf{E}\right) \odot \mathbf{R}_{\mathbf{S}}^{\mathrm{H}}\right)\right)^{-1} \tag{8}$$

where $\mathbf{P}_{\mathbf{G}} = \mathbf{I} - \mathbf{G}\mathbf{G}^{\dagger}$, $\mathbf{E} = [\mathbf{E}_1, \cdots, \mathbf{E}_K]$, $\mathbf{E}_k = \frac{d\mathbf{G}_k}{d\phi_k}$. $(\cdot)^{\mathrm{H}}$ and $(\cdot)^{\dagger}$ denote Hermitian transpose, and Moore-Penrose pseudo-inverse, respectively. $\mathbf{R}_{\mathbf{S}} = \mathrm{blkdiag}(\mathbf{R}_{\mathbf{S}_1}, \ldots, \mathbf{R}_{\mathbf{S}_L})$ is signal autocorrelation matrix and T is the snapshots of observation.

Next, we will show that CRB_{sub} is lower than CRB_{Ny} under the same conditions: the same array arrangement, same noise environment, and same snapshot($P = L$). Considering the expression of $\mathbf{G}$ and $\mathbf{E}$ and $\mathbf{B}^{\mathrm{H}}\mathbf{B} = \mathbf{I}$ when $P = L$, we hold

$$\begin{aligned}\mathbf{G}^{\mathrm{H}}\mathbf{G} &= \mathrm{blkdiag}\left(\mathbf{A}_1^{\mathrm{H}}\mathbf{A}_1, \cdots, \mathbf{A}_L^{\mathrm{H}}\mathbf{A}_L\right), \\ \mathbf{E}^{\mathrm{H}}\mathbf{E} &= \mathrm{blkdiag}\left(\mathbf{D}_1^{\mathrm{H}}\mathbf{D}_1, \cdots, \mathbf{D}_L^{\mathrm{H}}\mathbf{D}_L\right), \\ \mathbf{E}^{\mathrm{H}}\mathbf{G} &= \mathrm{blkdiag}\left(\mathbf{D}_1^{\mathrm{H}}\mathbf{A}_1, \cdots, \mathbf{D}_L^{\mathrm{H}}\mathbf{A}_L\right),\end{aligned} \tag{9}$$

where $\mathbf{D} = [(\mathbf{D}_1), \cdots, (\mathbf{D}_L)]$, $\mathbf{D}_l = [(\mathbf{D}_l)_1, \cdots, (\mathbf{D}_l)_{K_l}]$, $(\mathbf{D}_l)_k = \frac{d(\mathbf{A}_l)_k}{d\phi_k}$.

Further, based on (9) and after some matrix manipulations, we have

$$\mathrm{CRB}_{sub} = \mathrm{blkdiag}\left(\mathbf{C}_1, \cdots, \mathbf{C}_L\right), \tag{10}$$

where $\mathbf{C}_l = \frac{\sigma^2}{2T}\Re\left(\left(\mathbf{D}_l^{\mathrm{H}}\mathbf{P}_{\mathbf{A}_l}\mathbf{D}_l\right) \odot \mathbf{R}_{\mathbf{S}_l}^{\mathrm{H}}\right)^{-1}$. (10) shows that the new steer vectors corresponding to different subband would be completely uncorrelated in spite of that the primary steer vectors are correlated. This is the reason why once the sub-Nyquist sampling is employed, the performance of DOA estimation for any one subband is not affected by other subbands.

We consider the performance of DOA estimation in the following situations:

I) All of the signals are distributed in the lth subband and there is no signal in the other subbands. If the Nyquist sampling is employed, the CRB for the DOA in the lth subband is $\overline{\mathrm{CRB}}_{Ny}(l) = \frac{\sigma^2}{2T}\Re\left(\left(\mathbf{D}_l^{\mathrm{H}}\mathbf{P}_{\mathbf{A}_l}\mathbf{D}_l\right) \odot \mathbf{R}_{\mathbf{S}_l}^{\mathrm{H}}\right)^{-1}$.

II) The signals are distributed in not only the lth subband but also the other subbands. If the Nyquist sampling is employed, the CRB for the DOA in the lth subband is $\mathrm{CRB}_{Ny}(l)$.

III) The distribution of the signal is the same as II), but the sub-Nyquist sampling is employed. The CRB for the DOA in the lth subband is $\mathrm{CRB}_{sub}(l) = \mathbf{C}_l = \frac{\sigma^2}{2T}\Re\left(\left(\mathbf{D}_l^{\mathrm{H}}\mathbf{P}_{\mathbf{A}_l}\mathbf{D}_l\right) \odot \mathbf{R}_{\mathbf{S}_l}^{\mathrm{H}}\right)^{-1}$.

Based on section V of [20], the increase of the number of DOA will degrade the performance of DOA estimate, so we hold $\overline{\mathrm{CRB}}_{Ny}(l) \preceq \mathrm{CRB}_{Ny}(l)$. Further, we have

$$\mathrm{CRB}_{sub}(l) = \overline{\mathrm{CRB}}_{Ny}(l) \preceq \mathrm{CRB}_{Ny}(l). \tag{11}$$

(11) shows that when the signals are distributed in not only the lth subband but also the other subbands, in terms of the performance of DOA estimate for the signals in the lth subband, the method which employs sub-Nyquist sampling is better than the method which employs Nyquist sampling. Because l is arbitrary, $\mathrm{CRB}_{sub}(l) \preceq \mathrm{CRB}_{Ny}(l)$ is true for $1 \le l \le L$. So, we get

$$\mathrm{CRB}_{sub} \preceq \mathrm{CRB}_{Ny}, \tag{12}$$

the equality holds if and only if all of the signals are distributed in same one subband.

V. Simulation

In this section, the numerical simulations are carried out to study the performance with different source number. In the simulations, some complex-valued narrowband far-field non-coherent signals with equal power imping on a ULA composed of $M = 7$ sensors which are separated by a half wavelength corresponding to Nyquist sampling rate, which would probably be the signal highest frequency. We employ MRA to compress the signal in the spatial domain. The MRA is composed of $M = 7$ sensors which are located at $\mathbf{d} = [0, 1, 4, 10, 16, 22, 28]\, d$. We fix the number of snapshots at $T = 7000$ for Nyquist sampling, $T_{sub} = T/L$ for sub-Nyquist sampling, the Nyquist sampling rate at $f_N = 10$ GHz, the sampling rate reduction factor at $L = 7$, and the branch number at $P = L$. We set $\boldsymbol{\vartheta} = [\vartheta_1, \vartheta_2, \cdots, \vartheta_{14}]$, where ϑ_i follows the uniform distribution between -60° and 60°, where $1 \le i \le 14$. We set $\boldsymbol{\upsilon} = [\upsilon_1, \upsilon_2, \cdots, \upsilon_{14}]$, where $\upsilon_i, \upsilon_{i+7}$ are in the q_i-th subband, where $1 \le i \le L$, and $\{q_i\} = \{1, 2, \cdots, L\}$. We set DOA $\boldsymbol{\theta} = [\vartheta_1, \vartheta_2, \cdots, \vartheta_K]$ and frequency $\mathbf{f} = [\upsilon_1, \upsilon_2, \cdots, \upsilon_K]$. The definition of signal-to-noise ratio (SNR) and root-mean-square error (RMSE) of DOA is same as [20]. The SNR is fixed at 20 dB. 2000 Monte Carlo trials are implemented.

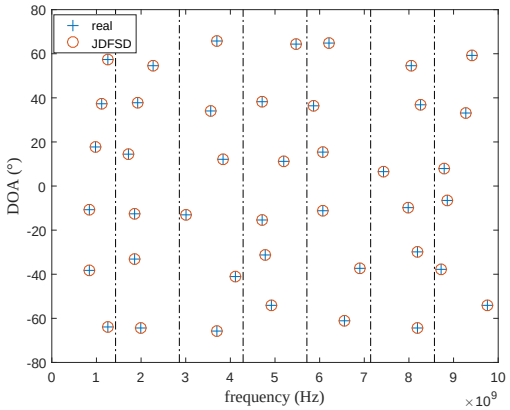

Fig. 1. Actual and estimated frequencies and their DOAs, maximum signal number $K = 42$ when $M = 7, P = L = 7$.

The first simulation will verify the estimation capacity. Based on section III, the maximum signal number which can be classified is $K = (M-1)L = 42$. Fig. 1 shows that the frequencies and DOAs can be accurately estimated when noise is free. The identical targets are at most $M - 1 = 6$ in each subband with $M = 7$ sensors.

As the analysis in part A of section VI in [20], the joint estimation performance is limited by the spatial phase or DOA estimation performance. Hence, only the spatial phase estimation performance is given in the simulation. Meanwhile, we will compare our methods with ST-Euler-ESPRIT in [18]. The receiver configuration parameters of ST-Euler-ESPRIT are the same as ours. The delay is Nyquist sampling interval $T_N = 1/f_N$. Fig.2 shows that the DOA estimation performances of algorithm JDFSD4MU is close to CRB_{sub} and lower than CRB_{Ny} except $K = 1$ whether ULA or MRA is employed. Apparently, when the MRA is employed, the spatial estimation performance is improved. When $K \le L$, CRB_{sub} and JDFSD4MU are not influenced by the signal number. When $K \ge L$, the traditional structure can not obtain the estimation of DOAs. However, our method still can achieve the estimation although the CRB_{sub} increases with signal number. The trend of $\mathrm{CRB}_{sub}(one)$ shows that increasing signal number only influences the estimation performance of the targets which are in the same subband, where $\mathrm{CRB}_{sub}(one)$ is the CRB of the DOA in the p_i-th subband. However, it does not happen to $\mathrm{CRB}_{Ny}(one)$. CRB_{Ny} increases with the signal number, and increases faster than exponential function of the signal number. Those meet the analysis in section IV. As for ST-Euler-ESPRIT, the RMSE increase with signal number and the performance is inferior to JDFSD4MU. ST-Euler-ESPRIT

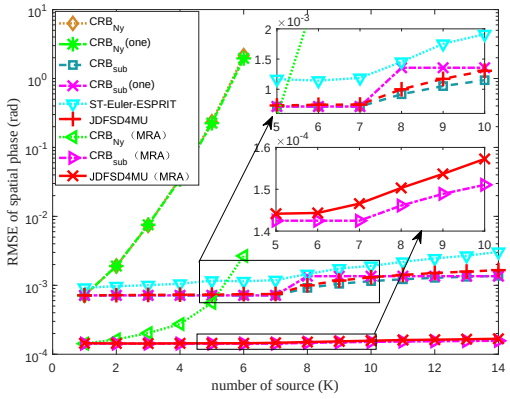

Fig. 2. RMSE of phase estimates versus number of source.

is limited by ULA, so the spatial estimation performance can not be improved by changing the array form as JDFSD4MU.

VI. Conclusions

In this letter, for the scenario where there may be more than one signal in a subband, by applying previous array receiver architecture and employing sub-Nyquist sampling techniques, we derived a more general time-space union model to jointly estimate frequency and DOA. We analyzed the identification of the model and gave the maximum signal number which can be classified so that the proposed model is capable to estimate more signals than sensors. We also proved that the CRB is lower than that employ Nyquist sampling. Furthermore, the simulation results verify the conclusions about the identification and CRB. Besides, the MRA can be employed to compress the signal in the spatial domain and improve the spatial estimation performance.

References

[1] S. Haykin, "Cognitive radio: brain-empowered wireless communications," *IEEE J. Sel. Areas Commun.*, vol. 23, no. 2, pp. 201–220, Feb 2005.

[2] T. Yucek and H. Arslan, "A survey of spectrum sensing algorithms for cognitive radio applications," *IEEE Commun. Surveys Tuts.*, vol. 11, no. 1, pp. 116–130, First 2009.

[3] M. Mishali and Y. C. Eldar, "Wideband spectrum sensing at sub-Nyquist rates [applications corner]," *IEEE Signal Process. Mag.*, vol. 28, no. 4, pp. 102–135, July 2011.

[4] H. Sun, A. Nallanathan, C. X. Wang, and Y. Chen, "Wideband spectrum sensing for cognitive radio networks: a survey," *IEEE Wireless Commun.*, vol. 20, no. 2, pp. 74–81, April 2013.

[5] D. Cohen and Y. C. Eldar, "Sub-Nyquist sampling for power spectrum sensing in cognitive radios: A unified approach," *IEEE Trans. Signal Process.*, vol. 62, no. 15, pp. 3897–3910, Aug 2014.

[6] H. Krim and M. Viberg, "Two decades of array signal processing research: the parametric approach," *IEEE Signal Process. Mag.*, vol. 13, no. 4, pp. 67–94, Jul 1996.

[7] R. Schmidt, "Multiple emitter location and signal parameter estimation," *IEEE Trans. Antennas Propag.*, vol. 34, no. 3, pp. 276–280, Mar 1986.

[8] R. Roy, A. Paulraj, and T. Kailath, "ESPRIT–a subspace rotation approach to estimation of parameters of cisoids in noise," *IEEE Trans. Acoust., Speech, Signal Process.*, vol. 34, no. 5, pp. 1340–1342, Oct 1986.

[9] A. N. Lemma, A. J. van der Veen, and E. F. Deprettere, "Joint angle-frequency estimation using multi-resolution esprit," in *Proc. IEEE Int. Conf. on Acous. Speech and Signal Process. (ICASSP)*, vol. 4, May 1998, pp. 1957–1960 vol.4.

[10] A. Lemma, A. J. V. der Veen, and E. Deprettere, "Analysis of joint angle-frequency estimation using esprit," *IEEE Trans. Signal Process.*, vol. 51, no. 5, pp. 1264–1283, May 2003.

[11] M. Mishali and Y. C. Eldar, "Sub-Nyquist sampling," *IEEE Signal Process. Mag.*, vol. 28, no. 6, pp. 98–124, Nov 2011.

[12] ——, "From theory to practice: Sub-Nyquist sampling of sparse wideband analog signals," *IEEE J. Sel. Topics Signal Process.*, vol. 4, no. 2, pp. 375–391, April 2010.

[13] Y. C. Eldar and T. Michaeli, "Beyond bandlimited sampling," *IEEE Signal Process. Mag.*, vol. 26, no. 3, pp. 48–68, May 2009.

[14] M. Mishali and Y. C. Eldar, "Blind multiband signal reconstruction: Compressed sensing for analog signals," *IEEE Trans. Signal Process.*, vol. 57, no. 3, pp. 993–1009, March 2009.

[15] D. D. Ariananda and G. Leus, "Compressive joint angular-frequency power spectrum estimation," in *Proc. Eur. Sig. Process. Conf. (EUSIPCO)*, Sep 2013, pp. 1–5.

[16] A. A. Kumar, S. G. Razul, and C. M. S. See, "An efficient sub-Nyquist receiver architecture for spectrum blind reconstruction and direction of arrival estimation," in *Proc. IEEE Int. Conf. on Acous. Speech and Signal Process. (ICASSP)*, May 2014, pp. 6781–6785.

[17] ——, "Spectrum blind reconstruction and direction of arrival estimation at sub-Nyquist sampling rates with uniform linear array," in *Proc. IEEE Int. Conf. Digital Sig. Process. (DSP)*, July 2015, pp. 670–674.

[18] A. A. Kumar, S. G. Razul, M. G. Chandra, C. M. See, and P. Balamuralidhar, "Joint frequency and direction of arrival estimation with space-time array," in *IEEE Sens. Array and Multichannel Signal Process. Workshop (SAM)*, July 2016, pp. 1–5.

[19] S. Stein, O. Yair, D. Cohen, and Y. C. Eldar, "Joint spectrum sensing and direction of arrival recovery from sub-Nyquist samples," in *Proc. IEEE Signal Process. Adv. Wireless Commun.(SPAWC)*, June 2015, pp. 331–335.

[20] L. Liu and P. Wei, "Joint DOA and frequency estimation with sub-Nyquist sampling," *arXiv preprint arXiv:1604.05037*, Apr 2016.